Design and Performance Evaluation of Transmitarray Lenses for Remote Cardiac Monitoring in the W-Band

Fitri Yuli Zulkifli
Antenna Propagation and Microwave Research Group, Department of Electrical Engineering, Faculty of Engineering, Universitas Indonesia, Indonesia
yuli@eng.ui.ac.id (corresponding author)

Adhirama Dwi Syaputra
Antenna Propagation and Microwave Research Group, Department of Electrical Engineering, Faculty of Engineering, Universitas Indonesia, Indonesia
adhirama.dwi@ui.ac.id

Aditya Inzani Wahdiyat
Antenna Propagation and Microwave Research Group, Department of Electrical Engineering, Faculty of Engineering, Universitas Indonesia, Indonesia
aditya.inzani31@ui.ac.id

Nurhayati Nurhayati
Department of Electrical Engineering, Faculty of Engineering, Universitas Negeri Surabaya, Surabaya, Indonesia
nurhayati@unesa.ac.id

Dewiani Djamaluddin
Department of Electrical Engineering, Faculty of Engineering, Universitas Hasanuddin, Makassar, Indonesia
dewiani@unhas.ac.id

Received: 13 January 2026 | Revised: 16 March 2026 and 12 April 2026 | Accepted: 17 April 2026

 DOI: https://doi.org/10.48084/etasr.17514

ABSTRACT

Non-contact radar offers a promising alternative to conventional electrocardiography for cardiac monitoring, yet its effectiveness is constrained by limited electromagnetic focusing capability toward deep cardiac structures. This paper presents transmitarray lenses operating in the 76–81 GHz band to enhance far-field focusing for radar-based cardiac sensing. A multi-layer unit cell with hexagonal split-loop topology is optimized to achieve 260.79° phase coverage and 75% transmission efficiency. Two lens apertures—8×8 and 16×16—are designed and evaluated in conjunction with a WR-10 horn antenna. Full-wave simulations incorporating biological tissue models demonstrate that both lenses preserve impedance matching while significantly increasing on-axis gain (16.5 dBi and 22.6 dBi, respectively) and concentrating electric field energy at the 50 mm cardiac depth. The 16×16 configuration achieves the sharpest focus with SAR levels well within IEEE safety standards. These results validate the feasibility of W-band transmitarray lenses for improving spatial resolution and detection accuracy in remote cardiac monitoring applications.

Keywords-transmitarray lens; W-band; wearable; radar; cardiac sensing; vital sign monitoring

I. INTRODUCTION

Wireless sensing technologies for medical telemonitoring have gained significant attention due to their ability to provide continuous and real-time cardiac observation, which is essential for early disease diagnosis [1]. Conventional cardiac monitoring techniques, such as Electrocardiogram (ECG), Photoplethysmogram (PPG), and Phonocardiogram (PCG), typically rely on direct skin contact through the placement of physical electrodes or sensors on the body, often leading to user discomfort, serving as a primary limitation for the applicability of wearable devices in long-term and ambulatory monitoring scenarios [2]. Radar-based sensing has emerged as an alternative approach, where micro-scale chest-wall vibrations induced by cardiac motion can be remotely detected using Doppler or Frequency-Modulated Continuous-Wave (FMCW) radar systems [3, 4].

Despite its potential, non-contact radar-based cardiac sensing faces a fundamental limitation in its ability to direct electromagnetic energy toward specific internal cardiac structures. Antennas operating at conventional microwave frequencies typically exhibit wide beamwidths and limited wavefront control, resulting in weak spatial selectivity and significant interference from surrounding tissues and environmental clutter [5]. This limitation becomes critical when attempting to sense deeper anatomical regions, where precise electromagnetic focusing is required to enhance signal-to-noise ratio and accurately extract heartbeat-induced micro-motions.

Transmitarray lenses provide an effective means of overcoming these limitations by enabling precise wavefront shaping using planar and compact metasurface structures. By engineering the transmission phase of subwavelength unit cells, transmitarrays can achieve high aperture efficiency, beamforming, and near-field focusing without the complexity of conventional phased arrays [6-8]. Recent studies have demonstrated that flexible and wearable transmitarray lenses can improve radar illumination and suppress clutter in vital-sign monitoring applications. In particular, a chest-worn transmitarray lens has been shown to enhance Inter-Beat Interval (IBI) estimation by focusing the radar beam toward the tricuspid valve region [9]. However, such implementations operate at relatively low frequencies, where the long wavelength inherently limits focusing sharpness and spatial resolution.

Operation in the 76–81 GHz millimeter-wave band offers distinct advantages for cardiac radar sensing. The short wavelength enables much tighter near-field focusing, while the wide contiguous bandwidth improves the discrimination of cardiac micro-motions from surrounding tissue movement [10]. Furthermore, antennas operating in this band inherently provide high directivity and stable radiation characteristics, and the spectrum is globally allocated for low-interference radiolocation applications [11]. Despite these advantages, the application of transmitarray lenses at 76–81 GHz for cardiac monitoring has not been reported in the literature. To address this challenge, this research proposes a transmitarray lens in the 76–81 GHz band that focuses incident radar energy towards the heart to enhance non-contact cardiac activity sensing. Biological tissues were involved in the simulation to more accurately replicate real-world operational conditions within the simulation environment. This comprehensive assessment examines focal intensity, spatial confinement, and penetration depth through anatomically accurate tissue layers, demonstrating the feasibility of high-resolution electromagnetic focusing for cardiovascular monitoring applications.

II. UNIT CELL DESIGN

The proposed transmitarray unit cell structure, shown in Figure 1, has a periodicity of W = 1.91 mm or 0.5 λ for 78.5 GHz. The unit cell comprises 4 identical metal layers and 4 substrate layers, where each metal and substrate layer is separated by an air gap of 1.085 mm to achieve the required transmission phase of 360°. The metal layer has a hexagonal split-loop pattern with loop width s = 0.1 mm, gap split g = 0.05 mm, and radius r. The unit cell with a hexagonal structure leads to the surface current flowing through a smooth path, which will cause a smaller variation in the input impedance and potentially achieve a wider bandwidth. The split gap is introduced to intentionally break the current continuity along the loop, thereby creating a localized capacitive discontinuity that enables the loop to resonate and provide a tunable phase response for the transmitarray unit cell. The substrate between the metal layers is made of Polymide (PI). It has a tangent loss ($\tan\delta$) of 0.0027, dielectric constant ε_r of 3.5, and thickness h of 0.9 mm.

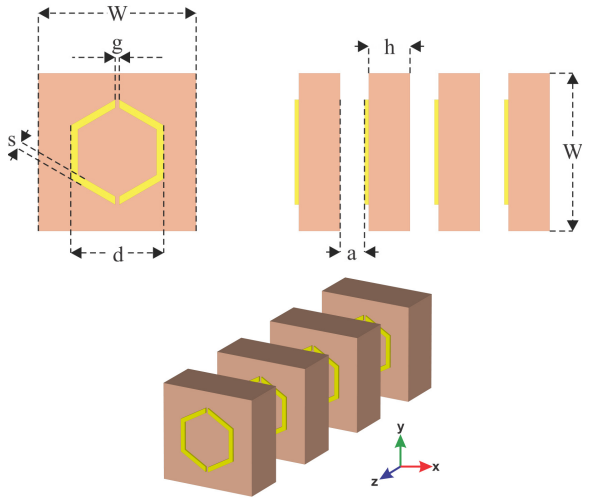

Fig. 1. Proposed unit cell design with 4 metal and substrate layers.

Figure 2 compares the S-parameters of the unit cell for 2-layer, 3-layer, and 4-layer configurations across the 50-100 GHz frequency range. As the number of layers increases, the transmission response S_{21} becomes smoother and exhibits deeper resonances near the target band, indicating improved coupling and phase-tuning capability. Meanwhile, the S_{11} parameter remains below -10 dB for a wider range of frequency span as the layer increases. These results show that a multi-layer architecture provides enhanced bandwidth and transmission performance, which are crucial for achieving the desired phase variation from the 76-81 GHz band.

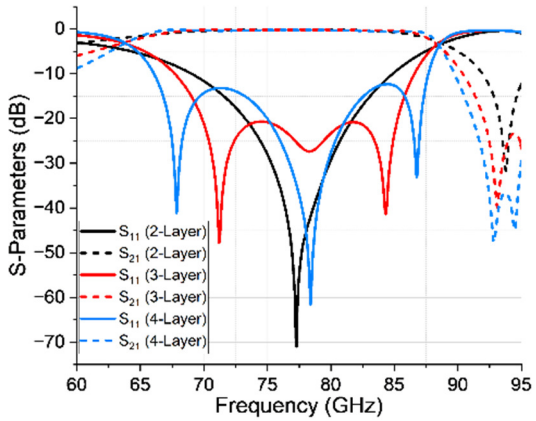

Fig. 2. S_{11} and S_{21} parameter comparison between 2-layer, 3-layer, and 4-layer unit cell designs.

The required transmission phase diversity is achieved by varying the hexagonal radius r from 0.1 to 0.44 mm for optimization. This work applies perfect electric and magnetic wall boundary conditions for the simulations. For the excitation of the unit cell, a normal incident plane wave was used in the simulation since the transmitarray lens will be located in the source antenna's far field region. Figure 3 illustrates the transmission coefficient correlation between the variation of hexagon radius and transmission coefficient, both in magnitude and phase. The graph shows that with variation of the hexagon radius from 0.1 to 0.44 mm, a minimum of 75% transmission efficiency and 260.79° phase range are achieved.

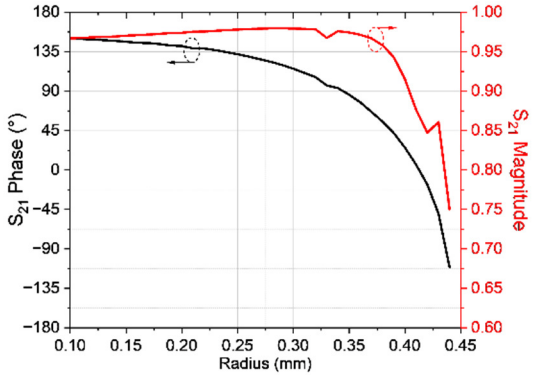

Fig. 3. Transmission phase and magnitude graph with radius variation.

III. TRANSMITARRAY LENS DESIGN AND FREE-SPACE RADIATION CHARACTERISTICS

To evaluate the impact of aperture size on the overall focusing performance, two transmitarray configurations were designed, a compact 8×8 array and a larger 16×16 array, as shown in Figure 4. The final design of the 8×8 array has a total length of 15.29 mm, while the 16×16 array has 30.576 mm. By comparing these two configurations under identical excitation and anatomical conditions, the analysis highlights how aperture scaling influences transmission efficiency, focal intensity, and beam confinement toward the targeted cardiac region. The phase distribution ϕ on the transmitarray lens to achieve a focusing effect can be calculated from:

$$\phi(r) = \frac{2\pi}{\lambda_0}\sqrt{r^2 + f^2} - f \quad (1)$$

where the coordinate system is defined with the origin (0, 0, 0) located at the geometric center of the transmitarray aperture.

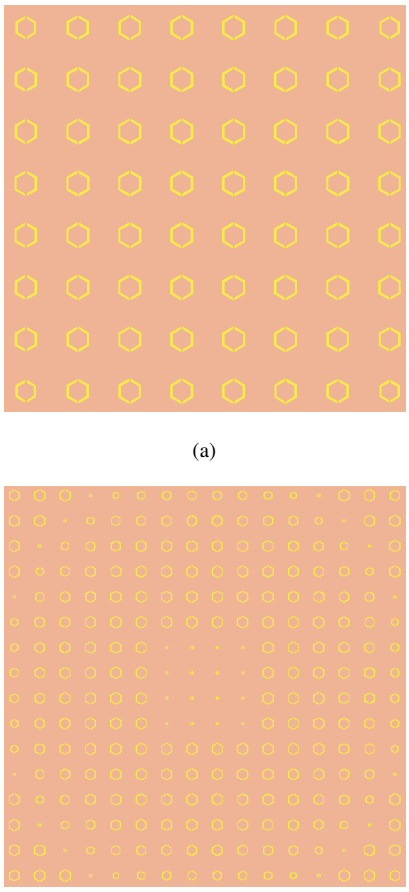

(a)

(b)

Fig. 4. Design of (a) 8 × 8 transmitarray and (b) 16 × 16 transmitarray.

The aperture plane coincides with the xy-plane at $z = 0$, where the unit cells are positioned. The focal point is located on the z-axis at $(0, 0, f)$, where f represents the focal distance. The transverse coordinates (x, y) denote the position of any unit cell within the aperture, and $r = \sqrt{x^2 + y^2}$ represents the radial distance from the aperture center. λ_0 indicates the free-space wavelength. The term $-f$ represents the reference phase, ensuring $\phi(0) = 0$ at the aperture center $(r = 0)$. Figure 5 illustrates the lenses' phase and magnitude distribution. A WR-10 waveguide horn antenna with $l_i \times w_i$ of 2.54×1.27 cm^2 and a thickness of 0.25 mm is used to feed both transmitarray lenses. The antenna is placed at a focal distance of 15 mm in front of the 8×8 array, resulting in an f/D value of ≈ 1. A similar f/D value applies to the 16×16 array, which has the focal distance of 30 mm. Figure 6 shows the geometric configuration of the transmitarray with the horn antenna. The radiation of the horn antenna will reach the lens after propagating as far as the focal length, before its phase is shifted to the desired phase for focusing purposes. To assess the electromagnetic wave performance after travelling through the

lens, this study compares the radiation pattern of a stand-alone horn antenna with that of a horn antenna equipped with both lenses, which is illustrated in Figure 7.

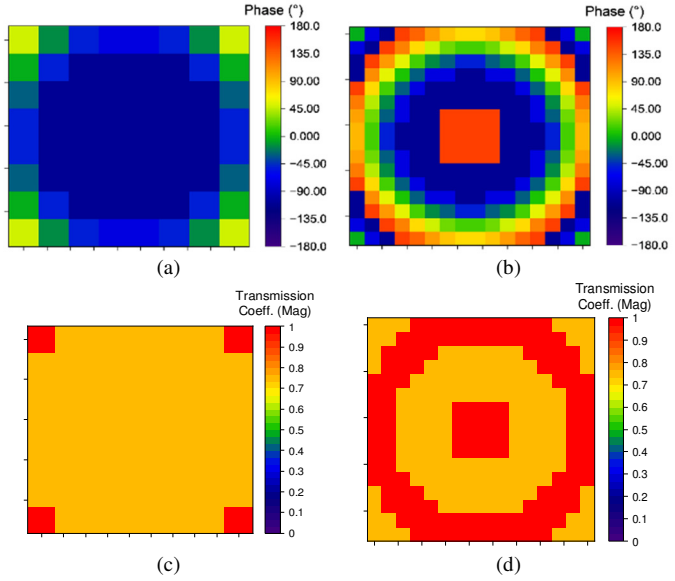

Fig. 5. (a) Phase distribution of the 8×8 array, (b) phase distribution of the 16×16 array, (c) magnitude distribution of the 8×8 array, and (d) magnitude distribution of the 16×16 array.

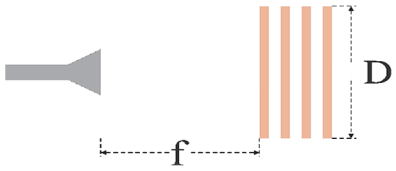

Fig. 6. Geometric configuration of horn feeder antenna with transmitarray.

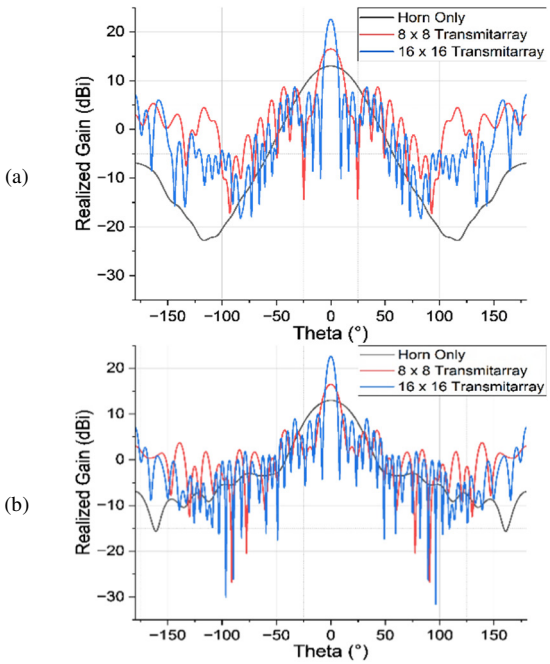

Fig. 7. Realized gain radiation pattern results of 3 scenarios: horn only, with 8×8 array, and with 16×16 array. (a) Phi 0° radiation pattern result; (b) Phi 90° radiation pattern result.

Figure 7 shows that the transmitarray gives noticeably higher gain in the broadside direction, demonstrating its ability to redirect and concentrate energy. With the horn only, 10 dBi of realized gain is achieved. With the 8×8 transmitarray, there is a 6 dBi of realized gain enhancement, achieving 16.5 dB. Moreover, the 16×16 transmitarray provides the strongest beam reinforcement and a narrower lobe, achieving a realized gain of 22.6 dBi.

IV. PERFORMANCE EVALUATION IN REALISTIC ENVIRONMENTS

To improve the fidelity and practical relevance of the simulation results, this research incorporated a multi-layer biological tissue model to evaluate the lenses' focal intensity, spatial confinement, and penetration depth in a realistic clinical scenario. The simulation setup represents a hospital room environment where the 16×16 transmitarray lens system is deployed for non-contact cardiac monitoring, as shown in Figure 8.

The system configuration consists of three main components arranged vertically. On the ceiling of the room, the WR-10 horn antenna is positioned to direct the electromagnetic energy downward. Below the horn antenna, the transmitarray lens is placed to shape and focus the incident wave. The electromagnetic wave propagates from the horn antenna through the transmitarray lens, where it undergoes phase shifting to achieve a narrow 7° Half Power Beam Width (HPBW). This focused beam then travels a distance of 2 m to reach the patient lying in a hospital bed. The 7° beamwidth results in 24 cm of energy dispersion and maximizes power delivery to the target region.

The 2-m propagation distance is specifically chosen to satisfy far-field criteria, ensuring that the 7° beamwidth remains stable and the wavefront approximates a plane wave across the thoracic region. The far-field boundary is defined as:

$$R_{ff} = 2D^2/\lambda \quad (2)$$

where D is the aperture size and λ is the wavelength. At 78.5 GHz, the 16×16 transmitarray requires an $R_{ff} \approx 0.49$ m. The 2-meter distance exceeds this threshold by more than fourfold, validating that the beam maintains its calculated divergence and provides uniform illumination at the patient location.

At the patient's thoracic region, the focused electromagnetic beam penetrates through three distinct biological tissue layers. The outermost layer is the skin, with a thickness of 10 mm and relative permittivity $\varepsilon_r = 34.09$. Below the skin lies the fat layer, with a thickness of 15 mm and $\varepsilon_r = 4.95$. The innermost layer is the muscle tissue, with a thickness of 25 mm and $\varepsilon_r = 47.71$. These tissue parameters are representative of human biological properties at W-band frequencies and provide an accurate model for electromagnetic wave propagation analysis. The total tissue thickness of 50 mm from the skin surface through the muscle layer corresponds to the typical depth at which the heart is located in the thoracic region.

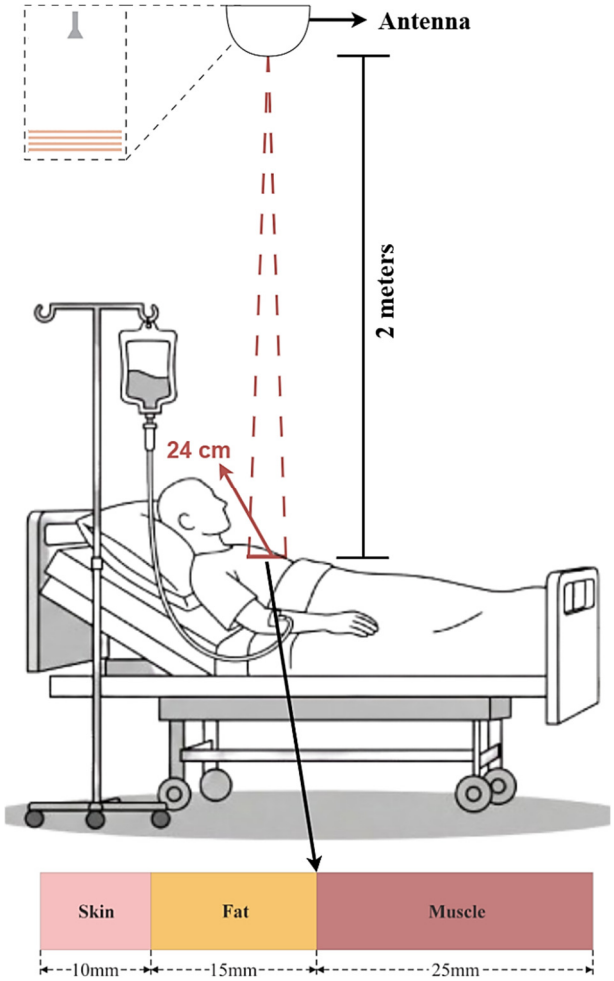

Fig. 8. Clinical deployment scenario showing the 16×16 transmitarray lens system positioned below the WR-10 horn antenna, with a multi-layer biological tissue model.

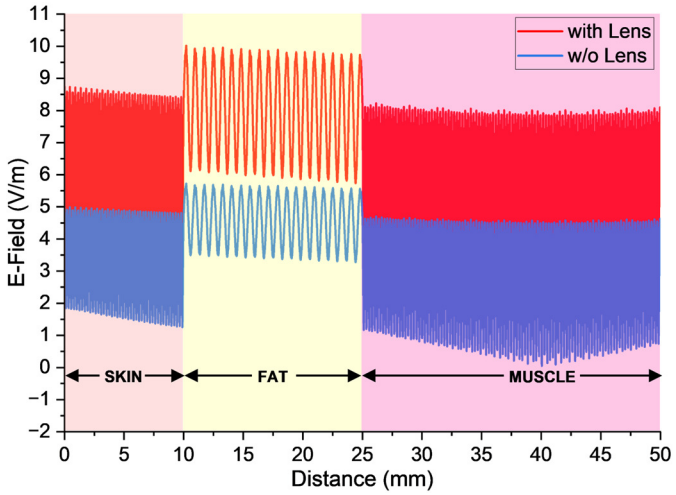

Fig. 9. E-Field distribution illustrating the focused beam propagation through the biological tissues, demonstrating concentration at the cardiac depth of 50 mm.

Figure 9 illustrates the comparative electric field strength distribution as electromagnetic waves propagate through multi-layered biological tissues, comparing the stand-alone WR-10 horn antenna (red trace) with the horn antenna integrated with a 16×16 transmitarray lens (blue trace). The horizontal axis represents the penetration depth from the skin surface (0 mm) to the muscle layer (50 mm), revealing the propagation characteristics across the three tissue interfaces.

The initial electric field at the skin surface (0 mm) is estimated from the electric field measured at the exit of the transmitarray lens located 2 m from the skin surface. Since the electric field magnitude is inversely proportional to the square of the propagation distance ($E \sim 1/r^2$), the estimated electric field at the skin surface is 8.46 V/m for the horn antenna without the transmitarray lens and 14.8 V/m when using the transmitarray lens. The 16×16 transmitarray lens achieves a sustained electric field enhancement across all tissue layers, with peak field strength of 10 V/m in the fat layer and 8.6 V/m at the 50 mm cardiac depth, compared to maximum values of 5.7 V/m and 4.9 V/m, respectively, for the stand-alone horn antenna. This field intensification confirms the capability of the lens to overcome tissue attenuation losses and deliver sufficient electromagnetic energy for non-contact cardiac monitoring applications.

The Specific Absorption Rate (SAR) was analyzed to evaluate the safety of electromagnetic exposure in biological tissues. SAR represents the rate at which electromagnetic energy is absorbed by biological tissue. Therefore, SAR analysis is important to ensure that the proposed system operates within acceptable exposure limits. SAR is calculated using the following expression:

$$SAR = \frac{\sigma E^2}{\rho} \quad (3)$$

where σ is the electrical conductivity of the tissue, E is the electric field magnitude, and ρ is the mass density. Based on the electric field data extracted from Figure 9, the resulting SAR value is 0.09 W/kg. This value is significantly lower than the allowable SAR limit specified in [12], which sets a maximum localized SAR of 1.6 W/kg for the torso.

V. CONCLUSION

Non-contact radar-based cardiac monitoring addresses the limitations of conventional contact-based electrodes; however, current systems still struggle with effective electromagnetic focusing toward deep cardiac structures. Existing research primarily relies on lower frequencies with limited spatial resolution, leaving a significant knowledge gap regarding the application of W-band (76–81 GHz) transmitarray lenses for cardiac sensing. This study fills this gap by developing a multi-layer hexagonal split-loop unit cell optimized to achieve a 260.79° phase range and 75% transmission efficiency. Key design steps involved evaluating 8×8 and 16×16 aperture configurations through full-wave simulations incorporating anatomically accurate multi-layer biological tissue models. Results demonstrate that the 16×16 configuration significantly enhances performance, achieving a realized gain of 22.6 dBi and a narrow 7° beamwidth compared to a standalone horn antenna at 10 dBi.

This research provides a novel demonstration of W-band transmitarray lenses that successfully concentrate electric field energy at a 50 mm cardiac depth—the typical location of the heart—through skin, fat, and muscle layers. Furthermore, the system ensures clinical safety with a calculated SAR of 0.09 W/kg, which is well below the IEEE maximum limit of 1.6 W/kg. These findings establish, for the first time, the feasibility of W-band transmitarray lenses for high-resolution, non-contact cardiac monitoring, providing a strong foundation for next-generation remote cardiovascular diagnostic systems.

DECLARATION OF COMPETING INTERESTS

Not applicable to this work.

ACKNOWLEDGMENT

This research was funded by Riset Kolaborasi Indonesia (RKI), Universitas Indonesia, under Grant No. PKS-627/UN2.RST/HKP.05/2025.

DATA AVAILABILITY

No dataset was used in this study. Simulation parameters are described within this paper.

REFERENCES

[1] M. Hamdani, M. Youcefi, A. Rabehi, B. Nail, and A. Douara, "Design and Implementation of a Medical TeleMonitoring System based on IoT," *Engineering, Technology & Applied Science Research*, vol. 12, no. 4, pp. 8949–8953, Aug. 2022, https://doi.org/10.48084/etasr.5040.

[2] R. A. I. Asyari, K. Y. Lee, R. E. Arif, T. S. J. Horng, and D. Teichmann, "A Novel Approach to Remote Detection in Medical Radar Applications Using Flexible Transmit Array Lenses," *IEEE Journal of Electromagnetics, RF and Microwaves in Medicine and Biology*, vol. 8, no. 1, pp. 36–50, Mar. 2024, https://doi.org/10.1109/JERM.2023.3347395.

[3] S. H. Zainud-Deen, W. M. Hassan, and H. A. Malhat, "Near-Field Focused Folded Transmitarray Antenna for Medical Applications," *Wireless Personal Communications*, vol. 96, no. 3, pp. 4885–4894, Oct. 2017, https://doi.org/10.1007/s11277-017-4433-7.

[4] R. E. Arif, M. C. Tang, W C. Su, T. S. Horng, F. K. Wang, and C. H. Tseng, "Designing a Metasurface-based Tag Antenna for Wearable Vital Sign Sensors," in *2019 IEEE MTT-S International Microwave Symposium (IMS)*, June 2019, pp. 373–376, https://doi.org/10.1109/MWSYM.2019.8700933.

[5] B. Nurzed, N. Saha, J. M. Millward, and T. Niendorf, "3D Metamaterials Facilitate Human Cardiac MRI at 21.0 Tesla: A Proof-of-Concept Study," *Sensors*, vol. 25, no. 3, Jan. 2025, Art. no. 620, https://doi.org/10.3390/s25030620.

[6] I. Derafshi and N. Komjani, "A New High Aperture Efficiency Transmitarray Antenna Based on Huygens Metasurfaces," *IEEE Transactions on Antennas and Propagation*, vol. 70, no. 7, pp. 5458–5467, July 2022, https://doi.org/10.1109/TAP.2022.3161480.

[7] A. H. Abdelrahman, F. Yang, A. Z. Elsherbeni, and P. Nayeri, *Analysis and Design of Transmitarray Antennas*. Springer International Publishing, 2017.

[8] X. Wang, M. S. Tong, and G. M. Yang, "Multifocus Multinull Near-Field Transmitting Focused Metasurface," *IEEE Transactions on Antennas and Propagation*, vol. 71, no. 4, pp. 3172–3182, Apr. 2023, https://doi.org/10.1109/TAP.2023.3240538.

[9] R. El Arif, W. C. Su, T. S. Horng, and C. T. M. Wu, "Chest-worn Transmitarray Lens for Monitoring Heart Rate Variability with a Remote Self-Injection-Locked Doppler Radar," in *2023 IEEE/MTT-S International Microwave Symposium - IMS 2023*, June 2023, pp. 1188–1191, https://doi.org/10.1109/IMS37964.2023.10188195.

[10] M. Ng Mou Kehn, E. Rajo-Iglesias, and T. Yang, "W-Band 76–81 GHz Millimeter-Wave Comb-Line Array for Automotive Short Range Radar," *Radio Science*, vol. 57, no. 4, Apr. 2022, Art. no. e2021RS007407, https://doi.org/10.1029/2021RS007407.

[11] "Coexistence between the radio astronomy service and radiolocation service applications in the frequency band 76-81 GHz," International Telecommunication Union (ITU), ITU-R RA.2457-0, June 2019.

[12] "IEEE Standard for Safety Levels with Respect to Human Exposure to Electric, Magnetic, and Electromagnetic Fields, 0 Hz to 300 GHz." IEEE, https://doi.org/10.1109/IEEESTD.2019.8859679.